Am J Physiol Regul Integr Comp Physiol 304: R929–R939, 2013.
First published April 3, 2013; doi:10.1152/ajpregu.00002.2013.

Detecting physiological systems with laser speckle perfusion imaging of the renal cortex

Christopher G. Scully,[1] Nicholas Mitrou,[2] Branko Braam,[3,4] William A. Cupples,[2] and Ki H. Chon[1]

[1]*Department of Biomedical Engineering, Worcester Polytechnic Institute, Worcester, Massachusetts;* [2]*Department of Biomedical Physiology and Kinesiology, Simon Fraser University, Burnaby, British Columbia, Canada;* [3]*Department of Medicine, University of Alberta, Edmonton, Alberta, Canada; and* [4]*Department of Physiology, University of Alberta, Edmonton, Alberta, Canada*

Submitted 2 January 2013; accepted in final form 30 March 2013

Scully CG, Mitrou N, Braam B, Cupples WA, Chon KH. Detecting physiological systems with laser speckle perfusion imaging of the renal cortex. *Am J Physiol Regul Integr Comp Physiol* 304: R929–R939, 2013. First published April 3, 2013; doi:10.1152/ajpregu.00002.2013.—Laser speckle perfusion imaging (LSPI) has become an increasingly popular technique for monitoring vascular perfusion over a tissue surface. However, few studies have utilized the full range of spatial and temporal information generated by LSPI to monitor spatial properties of physiologically relevant dynamics. In this study, we extend the use of LSPI to analyze renal perfusion dynamics over a spatial surface of $\sim 5 \times 7$ mm of renal cortex. We identify frequencies related to five physiological systems that induce temporal changes in renal vascular perfusion (cardiac flow pulse, respiratory-induced oscillations, baroreflex components, the myogenic response, and tubuloglomerular feedback) across the imaged surface and compare the results with those obtained from renal blood flow measurements. We find that dynamics supplied from global sources (cardiac, respiration, and baroreflex) present with the same frequency at all locations across the imaged surface, but the local renal autoregulation dynamics can be heterogeneous in their distribution across the surface. Moreover, transfer function analysis with forced blood pressure as the input yields the same information with laser speckle imaging or renal blood flow as the output during control, intrarenal infusion of N^{ω}-nitro-L-arginine methyl ester to enhance renal autoregulation, and intrarenal infusion of the rho-kinase inhibitor Y-27632 to inhibit vasomotion. We conclude that LSPI measurements can be used to analyze local as well as global renal perfusion dynamics and to study the properties of physiological systems across the renal cortex.

laser speckle imaging; renal autoregulation; tubuloglomerular feedback; myogenic response

AT LEAST FIVE DYNAMICS GENERATED by various physiological systems are present within renal blood flow, and measured perfusion signals can be used to study the systems and the interactions between them (9, 25). The five dynamics include global signatures generated outside the kidney, such as flow pulse representing the heart rate (HR), respiratory-induced oscillations (RO), and baroreflex components (BRC) generated in the mesenteric circulation (1), as well as the local renal autoregulation signatures generated within the renal vasculature, including the myogenic response (MR) and tubuloglomerular feedback (TGF). Each of the five systems operates within a distinct frequency range (Table 1), and with the use of spectral analysis the slower renal autoregulation signatures can be separated from the faster global signatures.

Address for reprint requests and other correspondence: K. H. Chon, Dept. of Biomedical Engineering, Worcester Polytechnic Institute, 100 Institute Rd., Worcester, MA 01609 (e-mail: kichon@wpi.edu).

Dynamics are identified in total renal blood flow (RBF) signals from transit time ultrasound measurements at the renal artery, in which the dynamics from ~30,000 nephrons are averaged together, or from single laser Doppler or tubule pressure recordings providing information from a single point on the surface or in a single nephron (15, 25, 27). However, it has been shown in experimental as well as modeling studies that nephron dynamics are not homogenous, and attributes of synchronization and coupling between nephrons are not considered when univariate measurements such as total RBF or tubule pressure are used (14, 21, 34).

Laser speckle perfusion imaging (LSPI) measures perfusion changes at points within an imaging window with high temporal and spatial resolution and has found success in imaging skin, cerebral, and renal vascular beds (4, 6, 12, 16). In LSPI, a speckle pattern is generated by imaging a laser-illuminated surface. Red blood cells act as scatterers and blur the pattern, allowing quantification of perfusion changes in the imaged region from the captured pixel statistics. Bezemer et al. (4) demonstrated that during occlusion of the renal artery, changes in RBF could be observed using LSPI, and spatial heterogeneity in renal perfusion was identified. Recently, there has been increasing interest in processing LSPI sequences to monitor dynamic changes in vascular perfusion signals (16). Analysis on single laser speckle signals has shown that time series extracted from individual pixels do not match those of laser Doppler flowmetry, but by increasing the number of pixels averaged to determine a perfusion index, the properties could become usable much the same way laser Doppler flowmetry has been used to monitor single-point dynamics (17, 18). Bricq et al. (6) showed the cardiac pulse in forearm blood flow could effectively be monitored within an LSPI imaging window by increasing the number of pixels averaged. In renal perfusion, Holstein-Rathlou et al. (14) investigated synchronization in TGF dynamics between LSPI signals extracted from nephron locations identified by imaging the vasculature.

In this study, we investigate if signals acquired from points on the renal cortex using LSPI contain information pertaining to renal perfusion dynamics beyond that acquired from RBF measurements in anesthetized rats. We hypothesize that dynamics related to the cardiac pulse, respiratory-induced oscillations, and baroreflex oscillations generated outside of the kidney will correlate with RBF and be homogenous across the renal cortex, whereas renal autoregulation dynamics will demonstrate spatial variance because they are generated locally. In addition, we compare transfer function analysis under forced blood pressure during intrarenal infusions to enhance and inhibit renal autoregulation.

Table 1. *Frequency bands for physiological systems*

	f_1, Hz	f_2, Hz
TGF	0.02	0.05
MR	0.1	0.3
BRC	0.35	0.7
RO	0.8	1.2
HR	4	7

Data are frequency bands (f_1, f_2) for tubuloglomerular feedback (TGF), myogenic response (MR), baroreflex component (BRC), respiratory oscillations (RO), and heart rate (HR).

MATERIALS AND METHODS

Experiments. All experiments were approved by the Animal Care Committee of Simon Fraser University, in accordance with the guidelines of the Canadian Council on Animal Care. Male Long-Evans rats (Harlan, Livermore, CA), ages 10–14 wk, were housed in pairs and given standard chow and distilled water ad libitum before the experiment. Twenty minutes before each experiment, the rat was given buprenorphine (0.02 mg/kg ip). Anesthesia was induced with 4% isoflurane in inspired gas (30% O_2, 70% air, 750 ml/min) and reduced to 2% thereafter. Animals were placed on a heated table (35°C) to maintain body temperature. The trachea was cannulated, and animals were ventilated with a small animal respirator (TOPO; Kent Scientific, Torrington, CT) operating in timed respiration mode and adjusted to match the natural breathing rate of each animal (~60 breaths/min). The left femoral vein was cannulated (PE-50) for infusion of saline containing 2% bovine serum albumin (1% body wt/h) to replace surgical volume losses. The left femoral artery was cannulated (PE-90 with narrowed tip) and connected to a pressure transducer (TRN050) and amplifier (TRN005; Kent Scientific) for blood pressure (BP) measurements. The left kidney was exposed by a subcostal flank incision. Once freed from surrounding fat, the kidney was mounted in a plastic cup anchored to the table. Stopcock grease (Dow Corning, Midland, MI) was placed in the cup to prevent motion and position the kidney toward the LSPI camera. The renal artery was stripped of fat and renal nerves. A Teflon cannula tip was inserted in the left femoral artery and then positioned in the renal artery for intrarenal infusions. RBF was measured with a transit time ultrasound flow probe (TS420; Transonic Systems, Ithaca, NY) mounted on the renal artery and secured with acoustic coupling gel (Surgilube and Nalco 1181). There was a 1-h postsurgery equilibration period during which the anesthetic concentration was reduced to ~1.5% or the lowest concentration that prevented responses to toe pinching.

Experiments were performed during spontaneous BP fluctuations ($n = 7$) and, on a separate set of animals, during broadband forcing of BP ($n = 8$). For the BP-forcing experiments, a motorized occluder was placed around the aorta above the left renal artery. The occluder was controlled by a program in Matlab, in the same manner as a previously reported system (25). The program drops renal perfusion pressure to a set pressure ~10% below spontaneous BP, and the pressure is then randomly changed by ±5% at 2-Hz iterations by adjusting the occluder throughout the forcing measurement period.

RBF and BP measurements were recorded continuously at 500 Hz. Twenty-five-minute LSPI measurements were made during control (CTL) conditions. Intrarenal infusion of the nonselective nitric oxide synthase inhibitor N^{ω}-nitro-L-arginine methyl ester (L-NAME; Sigma-Aldrich, Oakville, ON, Canada) was then initiated at 10 μg/min for 20 min, followed by 3 μg/min. After an ~25-min waiting period, another recording (L-NAME) was made. Next, the rho-kinase inhibitor Y-27632 (Cedarlane Laboratories, Burlington, ON, CA) (29) was infused intrarenally to achieve 10 μM in RBF (25), and after another ~25-min waiting period a final 25-min measurement (Y-27632) was made.

LSPI was performed with the moorFLPI laser speckle contrast imager (Moor Instruments, Axminster, UK) with an increased optical zoom and exposure time set to 2 ms. The moorFLPI illuminates the target surface with a 775-nm laser and captures the resulting speckle image with a 568 × 760-pixel charge-coupled device camera at a sampling rate of 25 Hz. The moorFLPI has the option of computing perfusion images by determining the statistics of a set of pixels over either temporal or spatial dimensions. We used a spatial set of pixels resulting in perfusion images sized 113 × 152 pixels at a sampling rate of 25 Hz (statistics computed for 5 × 5 squares of pixels at each frame). The moorFLPI translates the speckle contrast value into a relative perfusion unit termed flux. Assuming red blood cells are the primary source of motion in the kidney, a higher flux corresponds to increased velocity and/or concentration of red blood cells. Before each 25-min recording period, an ~4-mm hair was placed on the renal surface and the moorFLPI was positioned to include the full hair in the viewing window, resulting in the lens being ~20 cm from the renal surface. Recorded images of the hair were used to estimate the physical pixel size. A blackout curtain was positioned around the experimental area to block interference from ambient light.

Data analysis. moorFLPI sequences were loaded into Matlab r2011b (The MathWorks, Natick, MA), and a mask was drawn around any surface objects to ignore during analysis. To align LSPI sequences with RBF and BP measurements, RBF signals were low-pass filtered using a forward-backward noncausal filter to 12.5 Hz and downsampled to 25 Hz, matching that of the laser speckle signals. Laser speckle flux time-series from averaging all pixels at each frame (LS_{mean}) and RBF signals were then aligned by cross-correlation.

Identifying the physiological systems. For the data set recorded during spontaneous BP fluctuations, the power spectrum of the 25-Hz signals was computed using Welch's periodogram method with a 8,192-sample segment size and 50% overlap after linearly detrending the signals. Identification of the operating frequency of five physiological mechanisms was determined by finding the maximum amplitude from the power spectrum within the relevant frequency range (Table 1).

LSPI sequences were spatially filtered using a Gaussian filter ($\sigma = 3.12$), to improve signal-to-noise ratios at each pixel (6). The four exterior pixels around the edge of the image were removed after filtering because of edge effects caused by the filtering process. Because high-resolution spatial features are removed by the Gaussian filters, the filtered images were spatially down-sampled by a factor of 4, resulting in 27 × 37-pixel resized image sequences at 25 Hz. Power spectra of extracted time series from each pixel were computed and peak frequencies identified within each frequency region. This produced surface maps of the peak frequency at each pixel within each dynamic range. The coefficient of variation (CV) was computed as the standard deviation (σ) over the mean (μ) of the peak frequencies across the entire surface as a measure of surface heterogeneity. To account for variations in sizes of the five frequency bands, CV was normalized by the theoretical CV of a uniform distribution over each frequency band (f_1 to f_2) as derived in the APPENDIX (denominator in *Eq. 1*).

$$CV_{norm} = \frac{CV}{\frac{(f_2 - f_1)}{\sqrt{3}(f_2 + f_1)}} \quad (1)$$

A value of CV_{norm} close to 1 represents a uniform distribution of frequencies across the specified range.

The error of peak frequency estimates from LS_{mean} relative to RBF estimates was determined by computing the relative percent error between them (*Eq. 2*).

$$\text{Percent error} = \frac{|f_{LS} - f_{RBF}|}{f_{RBF}} \times 100 \quad (2)$$

Functional analysis. The data set recorded during broadband forcing of BP was used to characterize the functional aspects of renal

autoregulation. Signals were bandpass filtered between 0.004 and 1 Hz using a forward-backward noncausal elliptic filter and down-sampled to 2 Hz. Transfer function and mean-squared coherence estimates were computed using Welch's periodogram method with a 512-sample segment size and 50% overlap. Transfer functions were computed for each experiment with BP as the input and either RBF or LS_{mean} (spatial average at each frame) as the output.

To quantify functional aspects of renal autoregulation, four parameters were computed from the transfer function and coherence estimates. The mean coherence between 0.05 and 0.08 Hz was used as a measure of the nonlinearity between the flow and BP measurements (25). Mean gain in the low-frequency region (0.005–0.02 Hz) represents the ability of renal autoregulation to reduce BP fluctuations in the flow signals. The slope computed from 0.05 to 0.15 Hz represents the gain reduction from high to low frequencies, and the phase angle at 0.1 Hz describes the delay between frequencies in BP and those in flow signals at this frequency. Although the specific frequencies of operation may vary from animal to animal, we utilized strict frequency limits to perform pixel-by-pixel analysis from LSPI measurements.

Time-varying transfer functions. Time-varying transfer functions were determined with continuous wavelet transforms to determine temporal changes in renal autoregulation function. Signals were first passed through a 500-s moving average filter to remove slow changes in the mean during the infusions. The wavelet transform, $W(t, s)$ (*Eq. 3*), was found for both input (BP) and output (perfusion) signals by convolution with a zero-mean Morlet wavelet function, Ψ (*Eq. 4*), that is dilated across scales, s, and shifted across time. The Morlet wavelet was set with a center frequency, ω_o, of 6.

$$W(t, s) = \frac{1}{\sqrt{s}}\int_{-\infty}^{\infty} x(\tau)\psi^*\left(\frac{\tau - t}{s}\right)d\tau \quad (3)$$

$$\psi(t) = \pi^{\frac{-1}{4}} e^{i\omega_o t} e^{\frac{-t^2}{2}} \quad (4)$$

To compute transfer function characteristics, the cospectrum (*Eq. 5*) and quadrature spectrum (*Eq. 6*) were determined with W_X (input signal wavelet transform) and W_Y (output signal wavelet transform). An adaptive smoothing procedure was used to smooth the co- and quadrature spectra of the wavelet transforms (28). The cross-spectrum was determined using *Eq. 7*, and the time-varying transfer function, used to find system gain and phase angle, and the time-varying coherence function were determined using *Eqs. 8* and *9*, respectively (33).

$$CO_{XY}(t, f) = \text{real}\{W_X(t, f)W_Y^*(t, f)\} \quad (5)$$

$$QU_{XY}(t, f) = -\text{imag}\{W_X(t, f)W_Y^*(t, f)\} \quad (6)$$

$$W_{XY}(t, f) = CO_{XY} - iQU_{XY} \quad (7)$$

$$H_{XY}(t, f) = \frac{W_{XY}(t, f)}{W_X(t, f)} \quad (8)$$

$$C_{XY}(t, f) = \frac{|W_{XY}(t, f)|^2}{W_X(t, f)W_Y(t, f)} \quad (9)$$

Data are means ± SE. Statistical analysis was performed using SPSS Statistics 17.0. CV_{norm} values were compared using two-way repeated-measures ANOVA across experimental conditions and the five frequency bands. Differences in the transfer function parameters between infusion periods were analyzed with one-way repeated-measures ANOVA (with Greenhouse-Geisser correction if failed sphericity assumption). The Sidak post hoc test was used for pairwise comparisons ($P < 0.05$ considered significant).

RESULTS

With the 4-mm hair measurement, the size of a single pixel was measured as 37 ± 6 and 41 ± 3 μm on a side for the spontaneous and forcing data sets, respectively, and after spatial filtering and down-sampling, pixel sizes were 150 ± 9 and 163 ± 12 μm. The sizes of the imaged regions were ~4.2 × 5.6 and ~4.6 × 6.2 mm for the spontaneous and forcing data sets, respectively. A series of flux images is output from the moorFLPI, where the value at each pixel location is a relative perfusion index. Figure 1*A* shows an example renal perfusion image for the mean over the entire record at each pixel. High and low areas of perfusion can be identified, and high flux areas likely correspond to individual nephrons (14). Time series extracted from individual pixels contain significant noise (gray line in Fig. 1, *D* and *E*), but by averaging pixels together the noise can be reduced as shown by the blue line in Fig. 1, *D* and *E*, which corresponds to a 3 × 3-pixel average

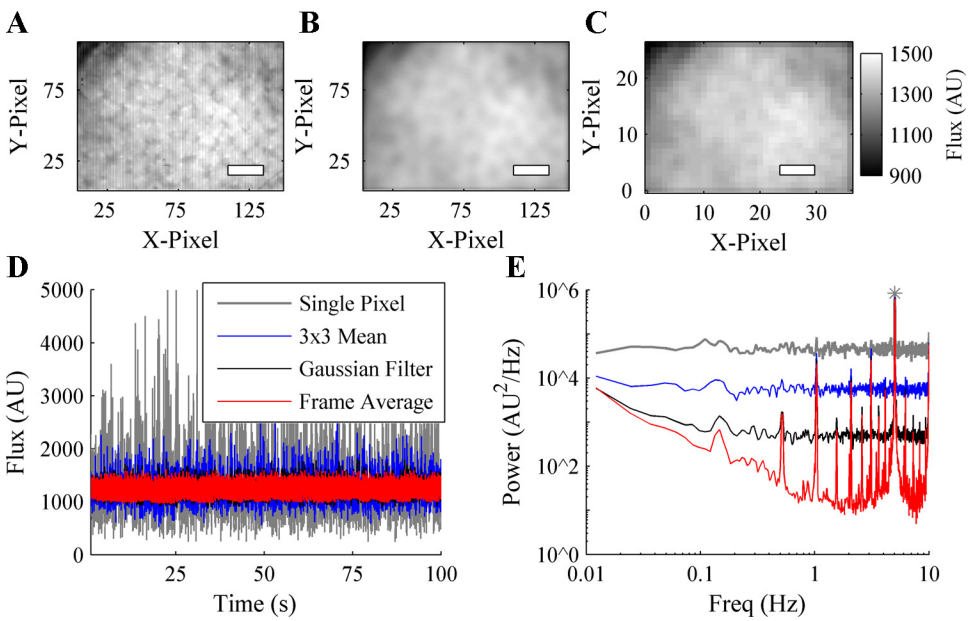

Fig. 1. *A*: flux image obtained by averaging the time series at each pixel. The white rectangle represents 1 mm in length. AU, arbitrary units. *B*: flux image after application of the Gaussian spatial filter at each frame. *C*: flux image after down-sampling of the spatially filtered series at each frame. *D*: 100 s of signals extracted from the flux image series. The gray line represents the time series extracted from a single pixel, the blue line is a 3 × 3-pixel average around the same pixel, the black line is the pixel time series after application of the spatial filter at each frame, and the red line is the average of all pixels within each frame. *E*: power spectra of the signals in *D*. Beyond the cardiac component (identified by the gray star on the single-pixel spectrum), no frequencies can be identified above the noise level from the time series extracted from the single pixel. Noise is reduced by taking a 3 × 3-pixel average, and further reduced with additional signals appearing after application of the Gaussian spatial filter. Noise continues to be diminished by averaging the entire frame.

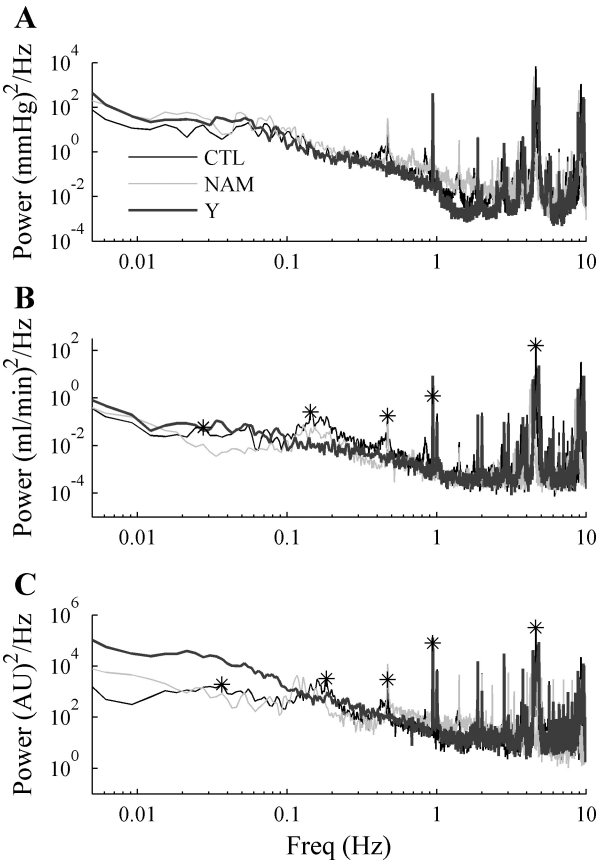

Fig. 2. Power spectra for blood pressure (*A*), renal blood flow (*B*), and laser speckle flux signals (*C*) acquired during control (CTL), N^{ω}-nitro-L-arginine methyl ester infusion (NAM), and Y-27632 infusion (Y). Five frequency peaks are denoted by stars on the CTL spectra for renal blood flow (RBF) and laser speckle flux (LS): the highest magnitude frequency (~5 Hz) corresponds to the cardiac pulse and at ~1 Hz is the frequency associated with respiratory oscillations. The peak at ~0.4 Hz corresponds to a baroreflex signature. Renal autoregulation mechanisms have frequencies at ~0.15 and ~0.03 Hz for the myogenic response (MR) and tubuloglomerular feedback (TGF), respectively. Peaks within the same frequency ranges can be identified in RBF and LS spectra.

(6). In the 3 × 3-pixel average the background noise across all frequencies is reduced, but the signatures of the dynamics are still buried within the noise. Figure 1*B* shows the same renal perfusion image as in Fig. 1*A* after the Gaussian spatial filter is applied across each frame, and the time series extracted from the same pixel have significantly reduced noise from the unfiltered perfusion series as well as the 3 × 3-pixel average (Fig. 1, *D* and *E*). The Gaussian spatial filter blurs the renal surface, so the series are down-sampled to reduce redundant analysis (Fig. 1*C*). Subsequent analysis performed on a pixel-by-pixel basis uses the down-sampled Gaussian spatial filter series. Single-signal analysis with LS_{mean} (red line in Fig. 1, *D* and *E*), was used to compare with RBF signals.

Identification of physiological components. Example spectra of total BP, RBF, and LS_{mean} are shown in Fig. 2, *A*, *B*, and *C*, respectively, during CTL, L-NAME, and Y-27632 conditions under spontaneous BP. Many frequencies can be identified from the signals, with respiratory-related oscillations (RO) and heart rate (HR) components at the high-frequency end (with respiration harmonics >1 Hz due to mechanical ventilation also present). Baroreflex components (BRC; ~0.4 Hz) (1) are present during CTL and L-NAME conditions in all three signals but are not present during Y-27632 infusion. Frequencies in the MR range (>0.1 Hz) appear only on the RBF and LS spectra during CTL and L-NAME and are not apparent after infusion of the rho-kinase inhibitor, showing that the MR is an active component in the renal vasculature. During Y-27632 infusion, low-frequency power increased, due to a lack of autoregulation. RBF and LS_{mean} spectra are similar in the high-frequency ranges containing the global parameters, but at the low-frequency band spectral differences exist in the MR and TGF characteristics.

Peak frequencies were identified for each region during CTL and L-NAME conditions; the Y-27632 period was not included since vasomotion was not apparent and no dominant frequency could be identified for TGF and the MR during this period. Identified frequencies from RBF and LS_{mean} were compared within each frequency range (Fig. 3). BRC, RO, and HR frequencies all showed high correlations, whereas renal autoregulation mechanisms identified in RBF and LS_{mean} did not correlate significantly in the identified operating frequencies. The percent error between the LS_{mean} and RBF estimates was determined for each frequency region over CTL and L-NAME conditions. Table 2 shows the median error for each frequency region. Median errors between the two signals are <1% for the BRC, RO, and HR estimates but much higher for TGF (33%) and the MR (25%) estimates.

With the use of the spatially filtered and down-sampled image series, power spectra were determined at each pixel location, and peak amplitudes within the five frequency ranges were determined and corresponding frequencies mapped back to their pixel location. This produced frequency surface maps as shown in Fig. 4, where the columns represent the five frequency regions and the rows represent the three infusion

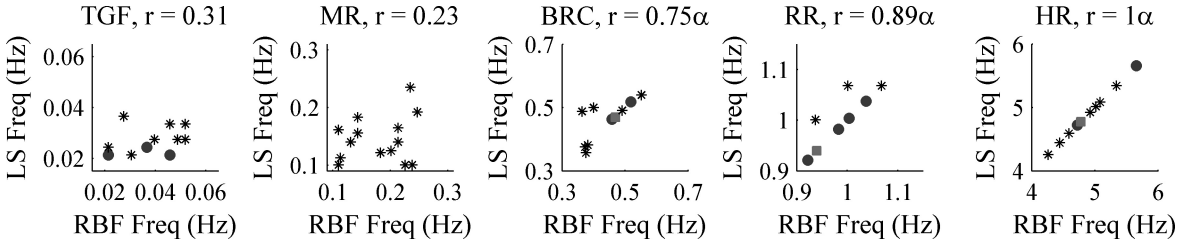

Fig. 3. Estimates of RBF and LS peak frequencies within each band during CTL and NAM (n = 14 for the 2 conditions). Overlapping data points are grouped together for visualization purposes: stars indicate unique data points, filled circles indicate 2 estimates at that location, and squares indicate 3 estimates at that location. Correlation coefficients (r) between the renal blood flow and laser speckle flux peak frequency estimates are presented for each frequency band. High correlations are identified from the cardiac pulse (heart rate, HR), respiration (RO), and baroreflex components (BRC). Frequencies identified in the MR and TGF ranges are not correlated between RBF and LS signals. α indicates significant correlation. Freq, frequency.

Table 2. *Peak frequency estimation error between laser speckle flux and renal blood flow*

	Median Error, % (10th, 90th percentiles)
TGF	33 (0, 53)
MR	25 (0, 56)
BRC	1 (0, 26)
RO	0 (0, 7)
HR	0 (0, 0)

Data are median peak frequency estimation errors for $n = 14$ experiments.

conditions. During all three conditions, RO and HR components were homogenous in their frequency distribution across the surface. The BRC frequency was constant for CTL and L-NAME. The BRC was not evident in the BP spectra in Fig. 2*A* during Y-27632 and therefore could not be identified in RBF or LS_{mean}. The MR and TGF both show heterogeneity in their frequency distribution during CTL and L-NAME. The MR frequency distribution appears random during Y-27632, because vascular smooth muscle activity is paralyzed and an MR signal can no longer be identified. During Y-27632, the TGF frequency map shows a frequency identified at 0.02 Hz, the low end of the TGF range, across much of the surface. Without vascular smooth muscle activity to generate a TGF component, there is increased spectral power at low frequencies in a 1/*f* manner, causing the lowest frequency within the TGF range to have the maximum amplitude.

To compare spatial heterogeneity between frequency regions, CV_{norm} was computed for each frequency surface during CTL and L-NAME conditions (Table 3). There was no significant difference in CV_{norm} between CTL and L-NAME. HR, RO, and BRC CV_{norm} values were all significantly lower than those of TGF and the MR, indicating a more heterogeneous distribution of frequencies for the renal autoregulation components.

Functional analysis of the renal autoregulation mechanisms. Transfer function plots using either total RBF or LS_{mean} as the output during BP forcing are shown in Fig. 5. Under CTL and L-NAME conditions, both sets of transfer functions show the hallmarks of renal autoregulation with system gain <0 dB at frequencies <0.05 Hz and increasing gain between $\sim$0.05 and 0.15 Hz (25, 31, 32). The phase angle was >0 rad between $\sim$0.02 and 0.1 Hz and dropped close to 0 rad in higher frequencies, indicating faster oscillations were not being altered by active elements within the kidney. Transfer function results are consistent with previously published reports showing impaired renal autoregulation after infusion of Y-27632 (9, 10, 25). Table 4 contains the parameters used to quantify autoregulation for both sets of transfer functions.

Supplemental Videos 1–3 show gain, coherence, and phase variations at each pixel over the range of frequencies from 0 to 0.5 Hz for CTL, L-NAME, and Y-27632 periods for one animal. (Supplemental data for this article is available online at the *American Journal of Physiology-Regulatory, Integrative and Comparative Physiology* website.) The four parameters in Table 4 were extracted from the transfer function at each pixel, and example surface maps of the parameters under each condition are shown in Fig. 6. The values are not constant across the renal surface, suggesting heterogeneity in renal autoregulation function within the imaged area.

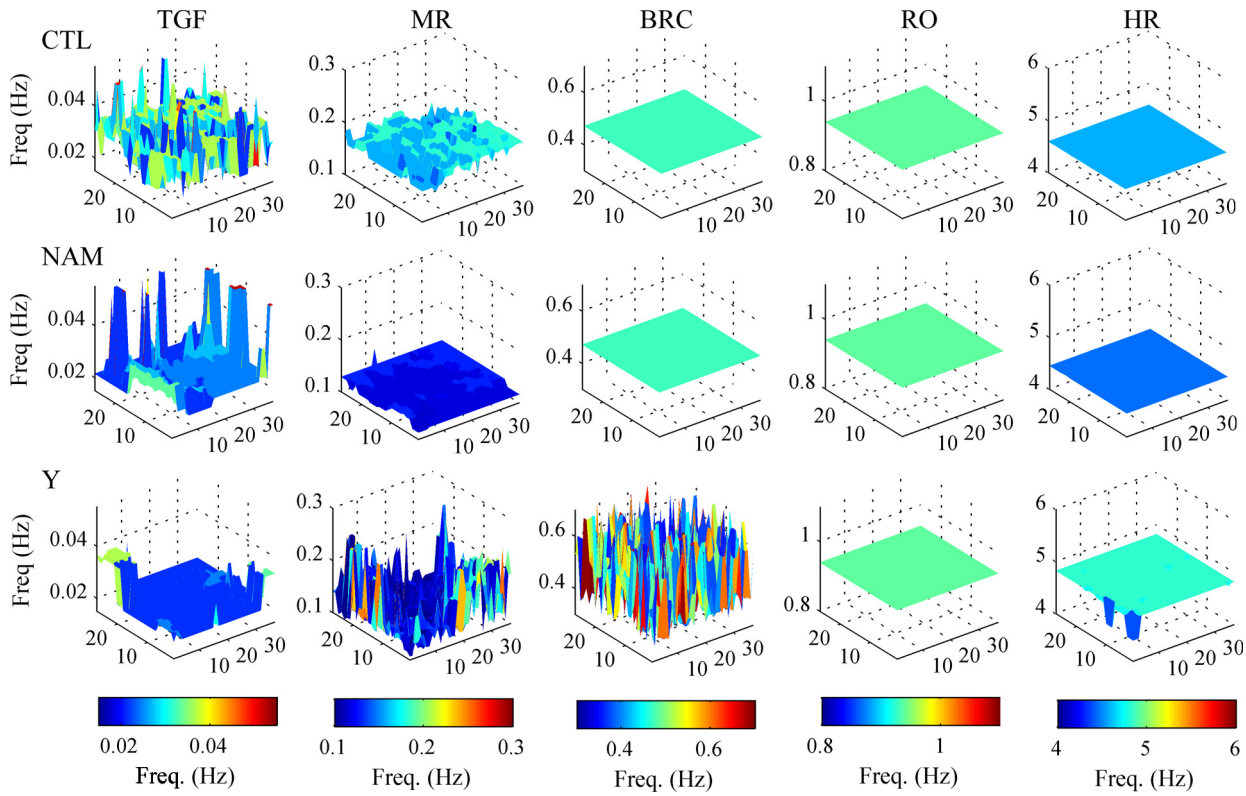

Fig. 4. Surface maps of the identified frequencies for the 5 regions during CTL (*top* row), NAM (*middle* row), and Y (*bottom* row) for 1 animal. In all cases RO and HR frequencies are consistent across the surface. The BRC is consistent during CTL and NAM but random during Y. MR and TGF frequencies are heterogeneous relative to the 3 global parameters during CTL and NAM. The *x*- and *y*-axes specify the pixel location after down-sampling.

Table 3. *Normalized coefficient of variations of surface frequency distributions*

	n	TGF	MR	BRC	RO	HR
$CV_{norm,}$ $\times 10^{-3}$						
CTL	7	202 ± 26	162 ± 27	108 ± 37	8 ± 8	1 ± 1
L-NAME	7	224 ± 30	207 ± 19	41 ± 25*†‡	4 ± 4*†‡	33 ± 18*†‡

Data are means ± SE of normalized coefficient of variation (CV_{norm}) during control (CTL) and N^{ω}-nitro-L-arginine methyl ester (L-NAME) infusions. *$P <$ 0.05, significantly different from TGF over the 2 conditions. †$P < 0.05$, significantly different from MR over the 2 conditions. ‡$P < 0.05$, significantly different from BRC over the 2 conditions. No significant difference existed between CTL and L-NAME.

Functional analysis was extended to monitoring system changes over time. Figure 7 shows the results for a forcing data set where two additional recording periods were made during initiation of L-NAME infusion and initiation of Y-27632 infusion. The signal traces (*top*) in Fig. 7 show LS_{mean} across the five monitoring periods as well as the BP recording throughout the experiment. Below the traces are time-varying transfer function characteristics for each period. As previously described (8), even under CTL conditions there are not consistent features, since nonstationarities occur throughout the recordings. System gain in the high-frequency region and phase angle in the low-frequency region both moderately increase during the CTL–L-NAME transition period and decrease along with an increase in coherence during the L-NAME–Y-27632 transition period.

The time-varying transfer functions were extended to the signals extracted from each pixel. Supplemental Videos 4 and 5 show changes at each pixel location in the transfer function parameters over time during CTL–L-NAME and L-NAME–Y-27632 transition periods. These videos demonstrate how functional renal autoregulation analysis can be extended from a single signal to both spatial and temporal dimensions and could allow identification of differences in the temporal response across a surface. Figure 8 shows transfer function analysis from three time points (150 s before and 100 and 350 s after initiation of intrarenal Y-27632 infusion) at two specific locations in the time-varying transfer function during the L-NAME–Y-27632 infusion period. The systems identified using the transfer functions are changing over time as Y-27632 is being infused, and active vasomotion is reduced in the vasculature at both locations.

DISCUSSION

We have shown that analysis of LSPI sequences provides insight into renal perfusion dynamics across spatial and temporal dimensions. LSPI captured cardiac, respiration, and baroreflex dynamics at all imaged locations, and high correlations were found between the frequencies identified in RBF and LS_{mean}. These are global parameters that are expected to occur throughout the cardiovascular system, so minimal differences

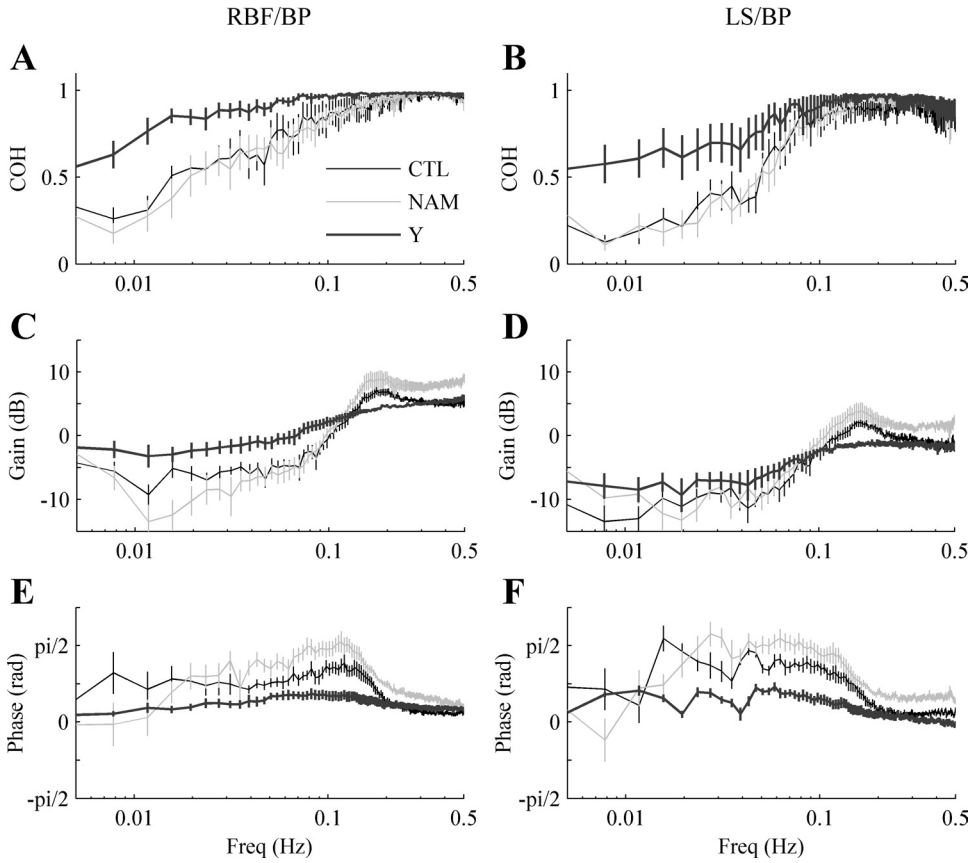

Fig. 5. Mean-squared coherence (Coh), transfer function gain, and phase angle computed for blood pressure as the input signal and RBF as the output signal are shown in *A*, *C*, and *E*, respectively ($n = 8$ for each condition). Transfer functions were also computed using the mean LS signal as the output in *B*, *D*, and *F*.

Table 4. *Transfer function parameters*

	n	BP, mmHg	$COH_{0.05–0.08\ Hz}$	$Gain_{0.005–0.02\ Hz}$, dB	$Slope_{0.05–0.15\ Hz}$, dB/decade	$Phase_{0.1\ Hz}$, rad
			Renal blood flow as output signal			
CTL	8	104 ± 3	0.78 ± 0.09	−6.6 ± 1.1	22.5 ± 3.2	1.08 ± 0.13
L-NAME	8	107 ± 3	0.72 ± 0.06	−10.2 ± 1.9	29.1 ± 4.1	1.50 ± 0.16
Y-27632	8	101 ± 6	0.95 ± 0.02†	−2.5 ± 1.2*†	10.3 ± 1.6*†	0.53 ± 0.10*†
			Laser speckle flux as output signal			
CTL	8		0.71 ± 0.08	−11.4 ± 1.9	22.1 ± 3.5	1.09 ± 0.16
L-NAME	8		0.68 ± 0.06	−11.2 ± 1.3	27.8 ± 6.7	1.36 ± 0.23
Y-27632	8		0.86 ± 0.07†	−8.0 ± 1.7	10.1 ± 3.2*†	0.47 ± 0.15*†

Data are means ± SE of blood pressure (BP), coherence (COH), low-frequency gain, gain slope reduction, and phase angle during CTL, L-NAME, and Y-27632 infusions. *$P < 0.05$, significantly different from CTL. †$P < 0.05$, significantly different from L-NAME.

between the frequency components in total RBF and extracted laser speckle signals are expected. The renal autoregulation components were identified in LSPI sequences, but their frequencies did not correlate with those in RBF measurements. RBF and LSPI are measuring perfusion from different anatomic locations, and an exact reproduction of what is found in RBF is not expected in LSPI. RBF is the average of ~30,000 nephrons (30), whereas LSPI, when averaged across the whole imaging window, may be looking at surface perfusion from ~100 nephrons, and when being considered on a pixel-by-pixel basis is providing information on a minimal number of local neighboring nephrons (14).

We found heterogeneity in the spatial distribution of dominant frequencies within the imaged region for renal autoregulation components but not the global parameters. CVnorm values of HR and RO are expected to be low, since they are global parameters that should present identically in the perfusion dynamics at all locations. Respiration was the most stable frequency across the surface as measured by CV_{norm} because animals were kept on mechanical ventilation at a fixed breathing rate. We found low variability in the baroreflex component between locations, suggesting identification of a single neurogenic source with no indication of local variations. This is expected since we performed renal denervation, because it has been shown that baroreflex oscillations present in renal blood flow are generated in the mesenteric circulation and baroreflex activity does not influence the renal blood flow dynamics (1, 19, 20). In contrast to the flow oscillations generated outside the kidney, TGF and the MR are local vasomotion operations that can be heterogeneous in their frequency distribution (14).

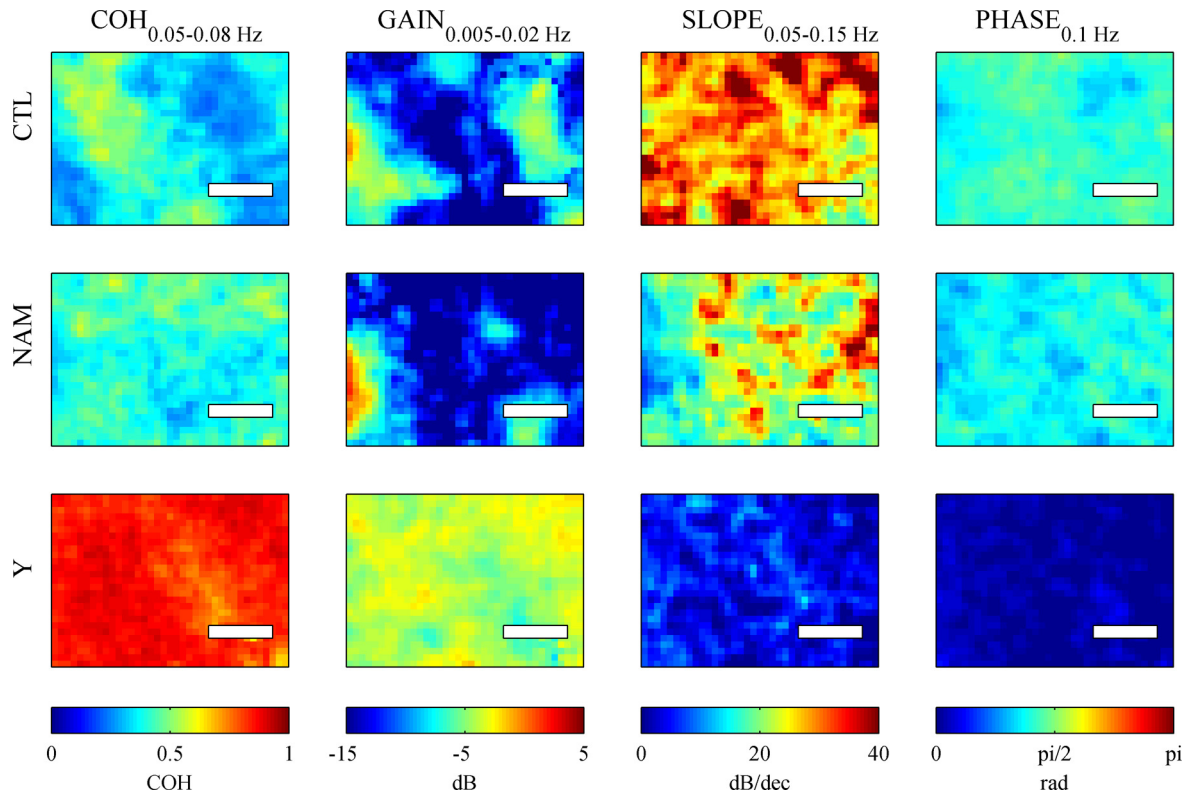

Fig. 6. Transfer function parameters at each pixel location during CTL (*top* row), NAM (*middle* row), and Y (*bottom* row) for 1 animal. The white rectangle represents 1.28 mm in length. Mean coherence from 0.05 to 0.08 Hz, low-frequency gain, gain slope reduction, and system phase at 0.1 Hz are shown in columns as indicated. dB/dec, decibels per decade.

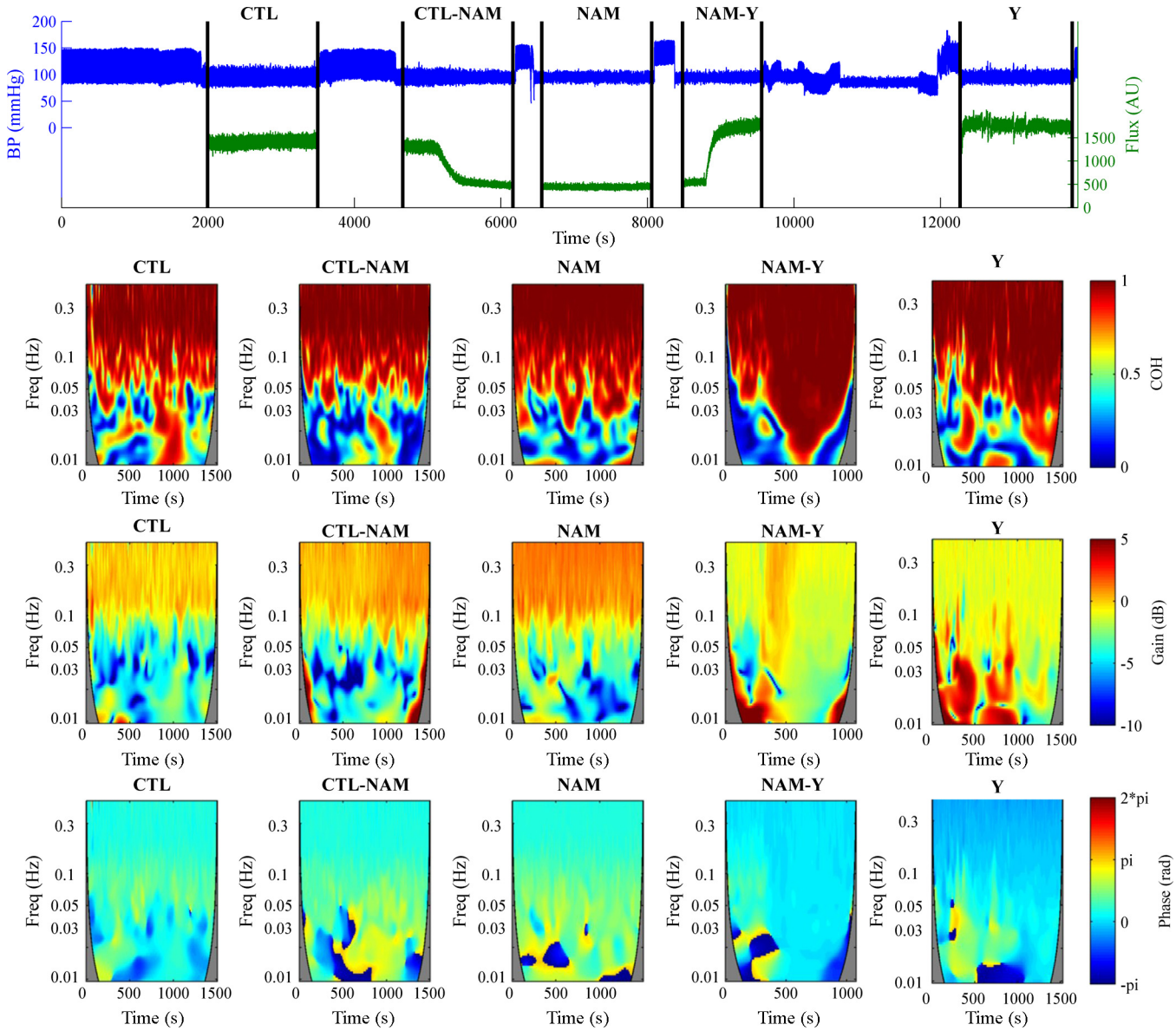

Fig. 7. Time-varying transfer function analysis of forcing data (including transition periods) The signal traces (*top*) show blood pressure (blue) and flux (green) signals over time; black vertical lines indicate the start and stop monitoring times for each of the 5 sections (CTL, CTL-NAM transition period, NAM, NAM-Y transition period, and Y). *Bottom*: time-varying coherence functions (*top* row), time-varying transfer function gain (*middle* row), and time-varying transfer function phase (*bottom* row) for each of the 5 periods. The gray area is the "cone of influence" caused by edge effects in the wavelet transform.

The MR and TGF showed variability in their frequency distribution across the surface relative to the three other components during CTL and L-NAME, but no dominant frequency could be identified for the renal autoregulation dynamics during rho-kinase inhibition due to an inability of vessels to contract (25).

Our transfer function results agreed with those of previous studies looking at the impact of intrarenal L-NAME and Y-27632 infusion on renal autoregulation (25). The shape in gain curves between RBF and LS_{mean} was similar, but gain using LS_{mean} as the input had an approximately −5-dB offset from that of RBF. This offset is probably caused by two confounding factors. BP fluctuations may already be somewhat damped when they reach the arteriolar level (13), resulting in an overestimate of the BP fluctuations compared with the local flow generating the laser speckle signal. Additionally, as with laser Doppler flowmetry, laser speckle imaging results in a non-zero flux signal under no-flow conditions (4, 22). Because of this offset in flux, we underestimate the fluctuations in LS_{mean}, resulting in a reduced gain at all frequencies. This offset is purely technical and does not affect the shape of the gain curves, phase angles, or coherence. Phase angles were also similar between RBF and LS_{mean} signals, telling us that the systems respond similarly to the changes induced by L-NAME and Y-27632 infusion, although the phase angle and coherence both decrease as the frequency approaches 0.5 Hz. This may be a result of imperfect timing between the laser speckle and BP recordings that were not synchronized through the instrumentation. This becomes evident at high frequencies, where a partial-second difference can have a significant impact on the phase angle between BP and laser speckle measure-

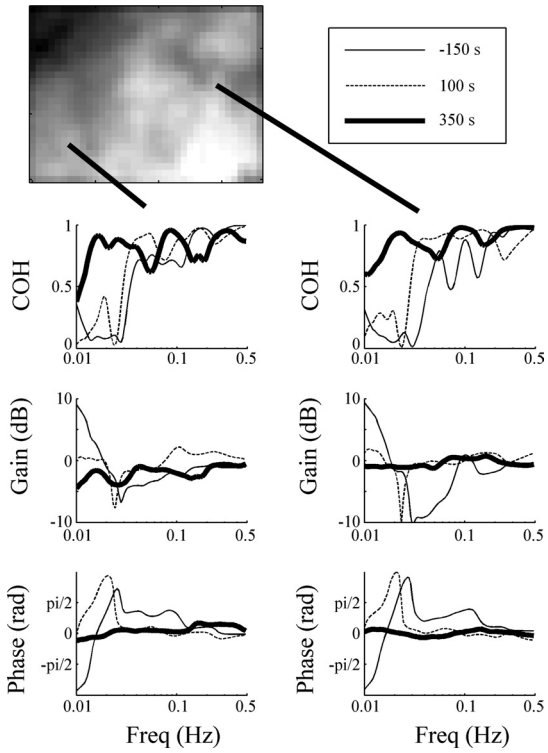

Fig. 8. Coherence, gain, and phase spectra at 2 different locations during the NAM-Y transition recording at 3 time points extracted from time-varying transfer functions. The time points are 150 s before, 100 s after, and 350 s after initiation of Y-27632 infusion. At 350 s after Y-27632 infusion has begun, coherence has increased in low frequencies, whereas gain and phase spectra have flattened at both locations. For any of the pairs of time points, the transfer functions from the 2 locations are similar but not identical.

ments. Whereas total RBF-based transfer functions describe how renal autoregulation is operating at the whole system level, the local LSPI data tell us how a subpopulation of superficial nephrons inside of the kidney is responding.

To quantify parameters, we used time-invariant frequency and transfer function analysis, but it has been shown that renal autoregulation dynamics are time varying (8, 11, 24). By applying time-varying transfer functions we can begin to study the response of these system properties over time, and from our Supplemental Videos we can visualize temporal as well as spatial changes. Figure 8 highlights how we are able to monitor changes in the transfer functions at all locations as Y-27632 impacts the system and we see the results of increased coherence and a flattened gain and phase spectra. This analysis could be used to understand how regions of nephrons in the renal cortex operate together, or independently, and what interventions might change these interactions.

Laser speckle imaging advantages and limitations. Laser Doppler flowmetry has previously been shown to be a successful method for analyzing renal autoregulation signals from a point on the renal surface containing information provided from tens to hundreds of nephrons (27, 30, 35). The advantage LSPI provides is that we are able to monitor perfusion at all locations across a surface simultaneously, which enables us to study the dynamics at all points (14). With a sampling rate of 25 Hz, the moorFLPI is capable of identifying frequencies up to the cardiovascular dynamics. Using an increased magnification moorFLPI system, we were able to have an imaging window of ~5 × 7 mm in size, allowing an extension of previous studies analyzing temporal signals in renal autoregulation that were limited to two or three simultaneous single-nephron measurements (7, 15, 34).

Studies have shown the importance of the number of pixels in computing accurate laser speckle statistics to obtain perfusion values (18, 26). The moorFLPI provides two options to compute perfusion values: temporally at each pixel over 25 frames (perfusion sequences sampled at 1 Hz) or spatially at each frame over a 5 × 5 region of neighboring pixels (perfusion sequences sampled at 25 Hz). In either mode, the number of pixels used for computation is fixed at 25. We used the spatial computation method to sample at a rate sufficient to capture the cardiac dynamics and avoid aliasing of cardiac and respiration components when analyzing renal autoregulation mechanisms. Single-pixel flux measurements of renal perfusion from the moorFLPI have low signal-to-noise ratios, and we therefore average flux values between neighboring pixels to receive adequate signals. This reduces our effective spatial resolution by the number of pixels averaged. To account for blurring introduced by the spatial filter, we downsample each frame by a factor of 4, increasing the physical width captured with each pixel from ~40 to ~160 μm/pixel. We are not able to identify specific nephrons using this method, but rather have cortical perfusion signals from locations across the renal surface.

A drawback to LSPI is that the depth of the tissue where blood flow is providing information is not precisely known (5, 23). LSPI has an advantage over laser Doppler in that the depth of imaging will be shallower even though LSPI generally uses a more powerful laser, because it uses a diverging laser source that spreads the power across the surface (23), whereas laser Doppler focuses the laser at a single location (30, 35). Depending on the specific instrument and area being imaged, the penetration depth for laser Doppler flowmetry may be at least three times greater than that for LSPI (23). In the highly vascularized renal cortex our predominant signal should be from scatterers (red blood cells) in the most superficial layers of the cortex (~100 μm deep) (4), which is ideal to examine blood flow in only the most superficial nephrons (2, 3). LSPI appears well suited for studying spatial and temporal variations in flow.

Perspectives and Significance

By performing functional analysis at points across the spatial imaged region, we are able to compare how renal autoregulation is functioning at multiple points in the superficial layer of the renal cortex, which has not been possible using traditional single point measurements. Holstein-Rathlou et al. (14) showed how this type of information can be used to understand the interactions between spatial locations. By using transfer function analysis across the renal surface, we have shown how this technology could be used to identify regions in the renal cortex that lack effective autoregulation. By visualizing the slope of gain reduction at all locations, we can see the systemic changes across the surface when the vasculature is unable to respond to BP fluctuations. By combining spatial perfusion imaging with time-varying analysis, we are able to determine which regions have properly functioning autoregulation and to track the system properties over time. This technique could be used to study the temporal response of the system under various conditions or potentially to identify regions of nephrons that may have failing autoregulation over time. This type of

analysis could be extended to other vascular beds to study vasomotion at many points within a region of interest.

APPENDIX

Coefficient of variation for a uniform distribution. The theoretical mean and standard deviation of a continuous uniform distribution over a band $[f_1, f_2]$ are defined as $\mu_{uniform}$ and $\sigma_{uniform}$ in *Eqs. A1* and *A2*, respectively.

$$\mu_{uniform} = \frac{(f_1 + f_2)}{2} \quad (A1)$$

$$\sigma_{uniform} = \sqrt{\frac{(f_2 - f_1)^2}{12}} \quad (A2)$$

The dimensionless coefficient of variation (CV) of a probability distribution is defined as the standard deviation over the mean (*Eq. A3*).

$$CV = \frac{\sigma}{\mu} \quad (A3)$$

Substituting the theoretical mean and standard deviation of a uniform distribution into *Eq. A3* produces the theoretical coefficient of variation of a uniform distribution (*Eq. A4*).

$$CV_{uniform} = \frac{(f_2 - f_1)}{\sqrt{3}(f_2 + f_1)} \quad (A4)$$

GRANTS

This work was supported by Canadian Institutes of Health Research Grant MOP-102694 (to W. A. Cupples, B. Braam, and K. H. Chon). C. G. Scully was supported by a predoctoral fellowship from the American Heart Association. B. Braam is a Heart and Stroke Foundation of Canada New Investigator.

DISCLOSURES

No conflicts of interest, financial or otherwise, are declared by the authors.

AUTHOR CONTRIBUTIONS

C.G.S., B.B., W.A.C., N.M., and K.H.C. conception and design of research; C.G.S. analyzed data; C.G.S., N.M., B.B., W.A.C., and K.H.C. interpreted results of experiments; C.G.S. prepared figures; C.G.S. and K.H.C. drafted manuscript; C.G.S., N.M., B.B., W.A.C., and K.H.C. edited and revised manuscript; C.G.S., N.M., B.B., W.A.C., and K.H.C. approved final version of manuscript; N.M. and W.A.C. performed experiments.

REFERENCES

1. **Abu-Amarah I, Ajikobi DO, Bachelard H, Cupples WA, Salevsky FC.** Responses of mesenteric and renal blood flow dynamics to acute denervation in anesthetized rats. *Am J Physiol Regul Integr Comp Physiol* 275: R1543–R1552, 1998.
2. **Beeuwkes R.** Efferent vascular patterns and early vascular-tubular relations in the dog kidney. *Am J Physiol* 221: 1361–1374, 1971.
3. **Beeuwkes R, Bonventre J.** Tubular organization and vascular-tubular relations in the dog kidney. *Am J Physiol* 229: 695–713, 1975.
4. **Bezemer R, Legrand M, Klijn E, Heger M, Post IC, van Gulik TM, Payen D, Ince C.** Real-time assessment of renal cortical microvascular perfusion heterogeneities using near-infrared laser speckle imaging. *Opt Express* 18: 15054–15061, 2010.
5. **Boas DA, Dunn AK.** Laser speckle contrast imaging in biomedical optics. *J Biomed Opt* 15: 011109–011112, 2010.
6. **Bricq S, Mahé G, Rousseau D, Humeau-Heurtier A, Chapeau-Blondeau F, Rojas Varela J, Abraham P.** Assessing spatial resolution versus sensitivity from laser speckle contrast imaging: application to frequency analysis. *Med Biol Eng Comput* 50: 1017–1023, 2012.
7. **Chen YM, Yip KP, Marsh DJ, Holstein-Rathlou NH.** Magnitude of TGF-initiated nephron-nephron interactions is increased in SHR. *Am J Physiol Renal Fluid Electrolyte Physiol* 269: F198–F204, 1995.
8. **Chon KH, Zhong Y, Moore LC, Holstein-Rathlou NH, Cupples WA.** Analysis of nonstationarity in renal autoregulation mechanisms using time-varying transfer and coherence functions. *Am J Physiol Regul Integr Comp Physiol* 295: R821–R828, 2008.
9. **Cupples WA, Braam B.** Assessment of renal autoregulation. *Am J Physiol Renal Physiol* 292: F1105–F1123, 2007.
10. **Cupples WA, Loutzenhiser RD.** Dynamic autoregulation in the in vitro perfused hydronephrotic rat kidney. *Am J Physiol Renal Physiol* 275: F126–F130, 1998.
11. **Cupples WA, Novak P, Novak V, Salevsky FC.** Spontaneous blood pressure fluctuations and renal blood flow dynamics. *Am J Physiol Renal Fluid Electrolyte Physiol* 270: F82–F89, 1996.
12. **Dunn AK, Bolay H, Moskowitz MA, Boas DA.** Dynamic imaging of cerebral blood flow using laser speckle. *J Cereb Blood Flow Metab* 21: 195–201, 2001.
13. **Heyeraas KJ, Aukland K.** Interlobular arterial resistance: influence of renal arterial pressure and angiotensin II. *Kidney Int* 31: 1231–1239, 1987.
14. **Holstein-Rathlou NH, Sosnovtseva OV, Pavlov AN, Cupples WA, Sorensen CM, Marsh DJ.** Nephron blood flow dynamics measured by laser speckle contrast imaging. *Am J Physiol Renal Physiol* 300: F319–F329, 2011.
15. **Holstein-Rathlou NH.** Synchronization of proximal intratubular pressure oscillations: evidence for interaction between nephrons. *Pflügers Arch* 408: 438–443, 1987.
16. **Humeau-Heurtier A, Abraham P, Durand S, Leftheriotis G, Henrion D, Mahé G.** Clinical use of laser speckle techniques: beyond the sole mapping. *Med Biol Eng Comput* 50: 1001–1002, 2012.
17. **Humeau-Heurtier A, Mahé G, Durand S, Abraham P.** Multiscale entropy study of medical laser speckle contrast images. *IEEE Trans Biomed Eng* 60: 872–879, 2013.
18. **Humeau-Heurtier A, Mahé G, Durand S, Henrion D, Abraham P.** Laser speckle contrast imaging: multifractal analysis of data recorded in healthy subjects. *Med Phys* 39: 5849–5856, 2012.
19. **Just A, Wittmann U, Ehmke H, Kirchheim HR.** Autoregulation of renal blood flow in the conscious dog and the contribution of the tubuloglomerular feedback. *J Physiol* 506: 275–290, 2004.
20. **Malpas SC, Evans RG, Head GA, Lukoshkova EV.** Contribution of renal nerves to renal blood flow variability during hemorrhage. *Am J Physiol Regul Integr Comp Physiol* 274: R1283–R1294, 1998.
21. **Marsh DJ, Wexler AS, Brazhe A, Postnov DE, Sosnovtseva OV, Holstein-Rathlou NH.** Multinephron dynamics on the renal vascular network. *Am J Physiol Renal Physiol* 304: F88–F102, 2013.
22. **Nilsson GE, Tenland T, Oberg PA.** Evaluation of a laser Doppler flowmeter for measurement of tissue blood flow. *IEEE Trans Biomed Eng* 597–604, 1980.
23. **O'Doherty J, McNamara P, Clancy NT, Enfield JG, Leahy MJ.** Comparison of instruments for investigation of microcirculatory blood flow and red blood cell concentration. *J Biomed Opt* 14: 034025–034013, 2009.
24. **Scully CG, Siu KL, Cupples WA, Braam B, Chon KH.** Time-frequency approaches for the detection of interactions and temporal properties in renal autoregulation. *Ann Biomed Eng* 41: 172–184, 2013.
25. **Shi Y, Wang X, Chon KH, Cupples WA.** Tubuloglomerular feedback-dependent modulation of renal myogenic autoregulation by nitric oxide. *Am J Physiol Regul Integr Comp Physiol* 290: R982–R991, 2006.
26. **Skipetrov SE, Peuser J, Cerbino R, Zakharov P, Weber B, Scheffold F.** Noise in laser speckle correlation and imaging techniques. *Opt Express* 18: 14519–14534, 2010.
27. **Smedley G, Yip KP, Wagner A, Dubovitsky S, Marsh DJ.** A laser Doppler instrument for in vivo measurements of blood flow in single renal arterioles. *IEEE Trans Biomed Eng* 40: 290–297, 1993.
28. **Torrence C, Webster PJ.** Interdecadal changes in the ENSO-Monsoon system. *J Clim* 12: 2679–2690, 1999.
29. **Uehata M, Ishizaki T, Satoh H, Ono T, Kawahara T, Morishita T, Tamakawa H, Yamagami K, Inui J, Maekawa M, Narumiya S.** Calcium sensitization of smooth muscle mediated by a Rho-associated protein kinase in hypertension. *Nature* 389: 990–994, 1997.
30. **Wang H, Siu K, Ju K, Moore LC, Chon KH.** Identification of transient renal autoregulatory mechanisms using time-frequency spectral techniques. *IEEE Trans Biomed Eng* 52: 1033–1039, 2005.
31. **Wang X, Cupples WA.** Interaction between nitric oxide and renal myogenic autoregulation in normotensive and hypertensive rats. *Can J Physiol Pharmacol* 79: 238–245, 2001.

32. **Wang X, Salevsky FC, Cupples WA.** Nitric oxide, atrial natriuretic factor, and dynamic renal autoregulation. *Can J Physiol Pharmacol* 77: 777–786, 1999.
33. **Whitcher B, Craigmile PF, Brown P.** Time-varying spectral analysis in neurophysiological time series using Hilbert wavelet pairs. *Signal Process* 85: 2065–2081, 2005.
34. **Yip KP, Holstein-Rathlou NH, Marsh DJ.** Dynamics of TGF-initiated nephron-nephron interactions in normotensive rats and SHR. *Am J Physiol Renal Fluid Electrolyte Physiol* 262: F980–F988, 1992.
35. **Yip KP, Holstein-Rathlou NH, Marsh DJ.** Mechanisms of temporal variation in single-nephron blood flow in rats. *Am J Physiol Renal Fluid Electrolyte Physiol* 264: F427–F434, 1993.